Fluid Phase Equilibria 378 (2014) 107–112

Contents lists available at ScienceDirect

Fluid Phase Equilibria

journal homepage: www.elsevier.com/locate/fluid

Hydrate nucleation in quiescent and dynamic conditions

Sheng Dai [a], Joo Yong Lee [b,*], J. Carlos Santamarina [c]

[a] National Energy Technology Laboratory, Morgantown, WV 26507, USA
[b] Korean Institute of Geoscience and Mineral Resources, Deajeon 305-350, Republic of Korea
[c] Geosystems Engineering, Georgia Institute of Technology, Atlanta, GA 30032, USA

ARTICLE INFO

Article history:
Received 19 February 2014
Received in revised form 16 June 2014
Accepted 7 July 2014
Available online 15 July 2014

Keywords:
Hydrate
Nucleation
Mechanical agitation
Interfacial tension

ABSTRACT

Gas hydrate nucleation is the spontaneous formation of an ordered crystalline lattice from a disordered phase. This inherently random process often involves long induction times particularly in quiescent conditions. An experimental study was conducted to explore the kinetics of hydrate formation in the presence of mineral grains and when subjected to mechanical agitation. Results show that tetrahydrofuran THF hydrate nucleation is facilitated in the presence of most minerals, and induction times are a function of mineralogy and surface characteristics. While mechanical vibration does not suppress the inherent stochastic nature of nucleation, mechanical agitation triggers nucleation when the imposed acceleration exceeds ~10 m/s^2.

1. Introduction

The nucleation of a new phase is the initial step in water freezing and hydrate formation. The spontaneous formation of an ordered crystalline lattice from a disordered phase is a random process [1]. In fact, a liquid can be "supercooled" beyond the solid phase equilibrium conditions without experiencing phase transformation. During this metastable state, small crystallites nucleate and immediately break apart. The induction time for decisive crystal growth can vary significantly and may extend for days when gas hydrate forms in quiescent conditions [2].

Continued crystal growth starts when nuclei exceed a critical size [1]. During phase transformation, the equilibrium temperature can be depressed by ionic concentration or capillary effects, due to the decrease in water activity [3]. Supercooling, induction time, and equilibrium temperature depression are graphically defined in Fig. 1 where the temperature signature corresponds to a fluid that undergoes exothermic phase transition during cooling.

While thermodynamic equilibrium conditions can be accurately predicted [4,5], the kinetics of hydrate formation depend on inherently stochastic nuclei formation [6–8]. Kinetics affects laboratory protocols, flow assurance [9], hydrogen storage [10], some forms of CO_2 sequestration and CO_2-CH_4 replacement [11,12]. The effects of sediment characteristics and externally imposed vibrations on hydrate nucleation are experimentally investigated in this study. A review of previous studies is presented first.

2. Previous studies

Nucleation is affected by thermal history, the type of solution, the presence and type of impurities, and agitation.

(1) Thermal history of the solution: The molecular structure of water that was previously part of hydrate may not be completely disordered when the PT conditions remain near the stability field. This memory effect reduces induction times for hydrate re-formation [13]. An order of magnitude increase in the cooling rate lowers the mean nucleation temperature by 0.6–2 °C [14].
(2) Physical properties of the solution: Viscosity and the amount of available mass affect nucleation and crystal growth [15]. Dissolved salts lower the activity of water through strong coulombic attraction as compared to the weaker hydrogen or van der Waals bonds in hydrate structures; lower activity requires lower temperature and higher pressure for phase equilibrium [3,5]. Other biological and polymeric inhibitors effectively hinder nucleation [16,17].
(3) Impurities: The presence of impurities favors heterogeneous nucleation and reduces both the induction time and the degree of supercooling as a function of particle surface characteristics [3,18–20]. On the contrary, small pore sizes shift the stability field to higher pressure or lower temperature [21–27].

* Corresponding author at: Korea Institute of Geoscience and Mineral Resources, 124 Gwahang-no, Yuseong-gu, Daejeon 305-350, Republic of Korea.
Tel.: +82 42 868 3219; fax: +82 42 868 3417.
E-mail address: jyl@kigam.re.kr (J.Y. Lee).

http://dx.doi.org/10.1016/j.fluid.2014.07.006
0378-3812/

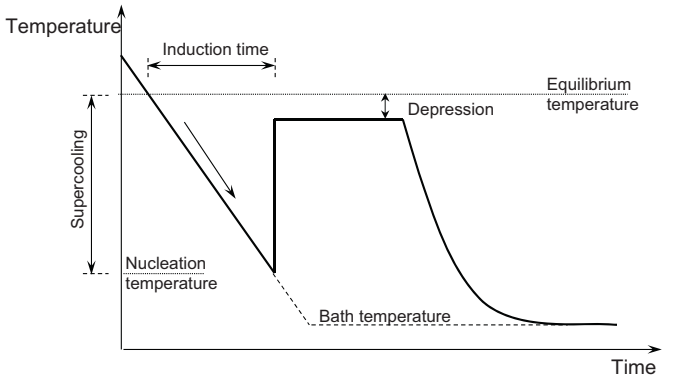

Fig. 1. Schematic temperature–time signature corresponding to an exothermic phase transformation during cooling—labels denote supercooling, induction time, freezing point depression, and equilibrium temperature.

(4) Mechanical agitation: Experiments show that stirring, shaking, or shocking can trigger nucleation in a supersaturated fluid [1,4,15,28,29]. Similarly, mechanical stimulation facilitates ice nucleation and gas hydrate formation [2,4,30,31]. Experimental results for other systems show that the nucleation rate and the morphology of precipitates are affected by stirring conditions and rate [20,32,33].

3. Experimental study

Two experimental studies are conducted to investigate the effect of minerals on THF (tetrahydrofuran) hydrate nucleation under quiescent conditions and to identify the characteristics of mechanical agitation that favor ice and THF hydrate formation. THF provides accurate control on hydrate saturation, overcomes the long diffusion-controlled formation time from aqueous phase and nucleates at atmospheric pressure; thus THF has been a popular proxy for methane in laboratory studies of hydrate-bearing sediment properties [34,35]. Devices and test procedures are described first.

3.1. Experimental devices and configurations

Fig. 2 illustrates the experimental configurations used for the two studies. Temperature is controlled using a high-precision cooler and measured using a smooth bar K-type thermocouple (precision of ~0.1 °C) for both static and dynamic tests. The temperature is measured at the tip of the thermocouple. In dynamic tests (Fig. 2b), external vibrations are supplied through a stainless steel rod (3.175 mm in diameter 100 mm in length) coupled to a piezoelectric actuator (Model 712A01, PCB Piezotronics, Inc.). Vibration frequency and amplitude are controlled through the power supply and the rod vibration is measured using a collinearly mounted accelerometer (Model 350B04, PCB Piezotronics, Inc.). The vibration frequency explored in this study ranges from 800 Hz to 7000 Hz, and the amplitude ranges from 1 nm to 1 μm.

3.2. Materials – specimen preparation

Specimens for static tests consist of 20 ml 81H_2O:19THF solution (stoichiometric solution—100% hydrate) and 5 g of soils. Table 1 summarizes the main properties of the selected soils. The randomly-shaped RP2 kaolinite is smaller than the hexagonal shaped SA1. Crushed silt is angular, low specific surface silt. Precipitated silt consists of silt-size aggregations with extensive inter-particle pore networks which result in high specific surfaces.

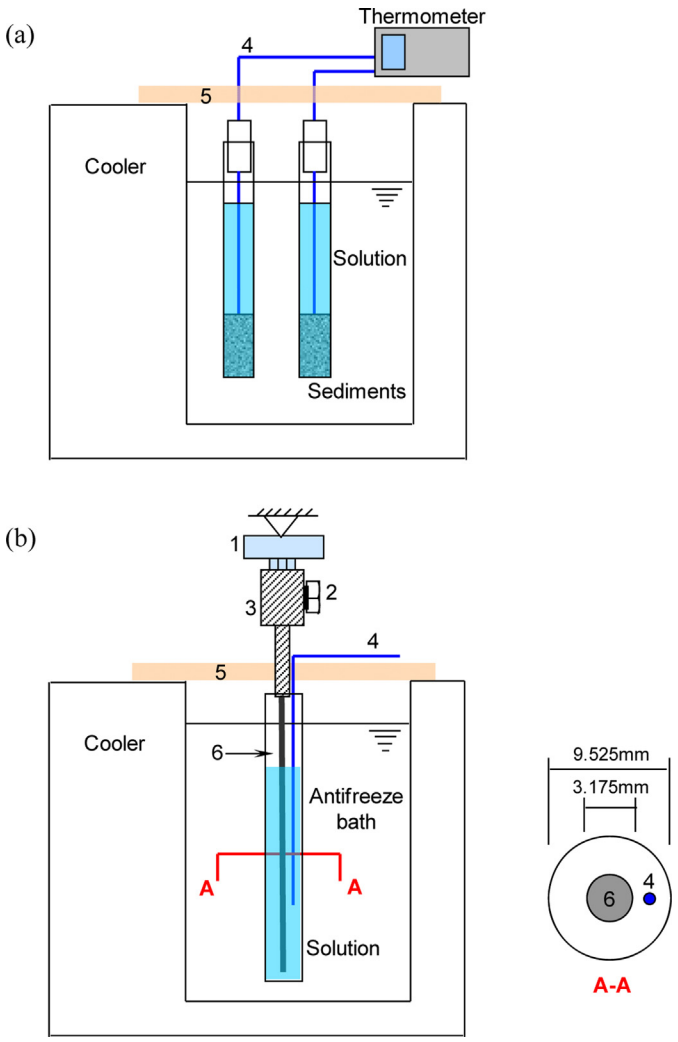

Fig. 2. Experimental configuration: (a) static test and (b) vibration test. Components: 1. Piezoelectric actuator (Model 712A01, PCB Piezotronics, Inc.). 2. Accelerometer (Model 350B04, PCB Piezotronics, Inc.). 3. Nylon coupler. 4. Thermocouple (K-type, precision = 0.1 °C). 5. Heat-insulation foam cover. 6. Stainless steel rod (100 mm in length).

The irregularly shaped GCC particles are bulkier than the very uniform, rice-shaped PCC particles.

The selected soil is added to the solution, shaken vigorously, and left to rest in the sealed cylinder for 1–2 h to allow for sedimentation. A thin layer of oil is added to cover THF solution specimens immediately after mixing to prevent THF evaporation during testing. Each test starts with a freshly prepared specimen to avoid contamination or memory effects.

Dynamic tests involve either 10 ml deionized water (ice formation) or 10 ml 19H_2O:81THF stoichiometric solution (100% hydrate formation).

3.3. Experimental procedures

Prepared specimens in test cylinders are sealed and immersed into a cooling bath with a constant temperature of −5 °C. In dynamic tests, the oscillatory vibration with preselected frequency and amplitude is applied immediately after the cylinder is submerged in the cooler. Bath and specimen temperatures are monitored to detect phase transformation.

Table 1
Physical properties of selected sediments.

	Kaolinite (SA1)	Kaolinite (RP2)	Precipitated silt (PS)	Crushed silt (CS)	Ground $CaCO_3$ (GCC)	Precipitated $CaCO_3$ (PCC)
Specific gravity, *Gs*	2.6	2.6	2.08	2.65	2.71	2.71
Mean grain size, d_{50} [μm]	1.1	0.36	20	20	12	1
pH	6.5	4.66	7	7	8.76	9.87
Specific surface, S_s [m^2/g]	36	29	120	0.113	1.8	9.9
Liquid limit, *LL*	43	78	–	–	28	52
Sphericity, *S*	0.7	0.7	0.9	0.9	0.8	0.2
Roundness, *R*	0.1	0.3	0.7	0.1	0.5	0.9

3.4. Typical temperature signatures

The equilibrium temperature at the THF hydrate boundary depends on the volume fraction of water and THF (Fig. 3a). At atmospheric pressure, the equilibrium temperature of $81H_2O$:19THF solution is ~4.5 °C. Typical temperature–time signatures of deionized water, excess water THF solution ($90H_2O$:10THF), stoichiometric mixture ($81H_2O$:19THF), and excess THF solution ($40H_2O$:60THF) are shown in Fig. 3b. The induction time in these signatures varies from 3000 s (water) to more than 6000 s (excess water solution). Supercooling reaches −7.5 °C (stoichiometric solution). The exothermic peak readily seen in all cases marks the beginning of the transformation. All reactions reach the equilibrium temperature. The excess water solution exhibits the exothermic peak for hydrate formation followed by the peak for ice formation.

4. Results and analyses

4.1. Heterogeneous hydrate nucleation—static tests

A total of 40 static tests were completed as part of this study. Results are summarized in Fig. 4. Measured induction times are log-normally distributed (note: a log-normal distribution of induction times was also observed in CO_2 hydrate nucleation in Na-montmorillonite suspensions [8]). The presence of minerals facilitates nucleation, except in the case of precipitated calcium carbonate PCC. Industrial precipitated mineral (PCC and PS) are less effective at nucleating hydrates than their crushed counterparts (GCC and CS); industrial minerals also exhibit higher water–mineral contact angle.

Mineral surfaces lower the thermal agitation of water molecules, and prompt their alignment; hence, mineral surfaces that more closely mimic the hydrate crystal structure are more efficient nucleators [36–38]. The number of water molecules per unit volume next to mineral surfaces n_w ($1/m^3$) can be estimated in terms of porosity *n* and specific surface S_s (m^2/g):

$$n_w = \frac{S_s(1-n)\ G_s\rho_w}{(l_{\text{water}})^2} \quad (1)$$

where G_s is specific gravity of minerals, ρ_w is water density, and l_{water} is the characteristic length of a water molecule (estimated n_w for each specimen based on the above equation are SA1: $180/m^3$, RP2: $145/m^3$, PS: $600/m^3$, CS: $0.565/m^3$, GCC:$9/m^3$, and PCC: $49.5/m^3$). Experimental results in Fig. 4 do not show clear benefits from specific surface (highest for the two kaolinite clays), implying that specific surface is less important than other mineral surface characteristics including roughness In fact, the rate of nucleation has been linked to the Gibbs free energy ΔG^*, which can be linked to contact and interfacial tension [14].

Sediment pores can also affect nucleation kinetics in various ways, particularly as pore sizes become smaller than 10 nm [21,23,25,26]: nanometer-sized pores restrict embryo size, water activity is reduced, and capillary suction hinders nucleation (multiphase fluids). Pore sizes in this study are 100 nm or larger and exert minimal effects on nucleation.

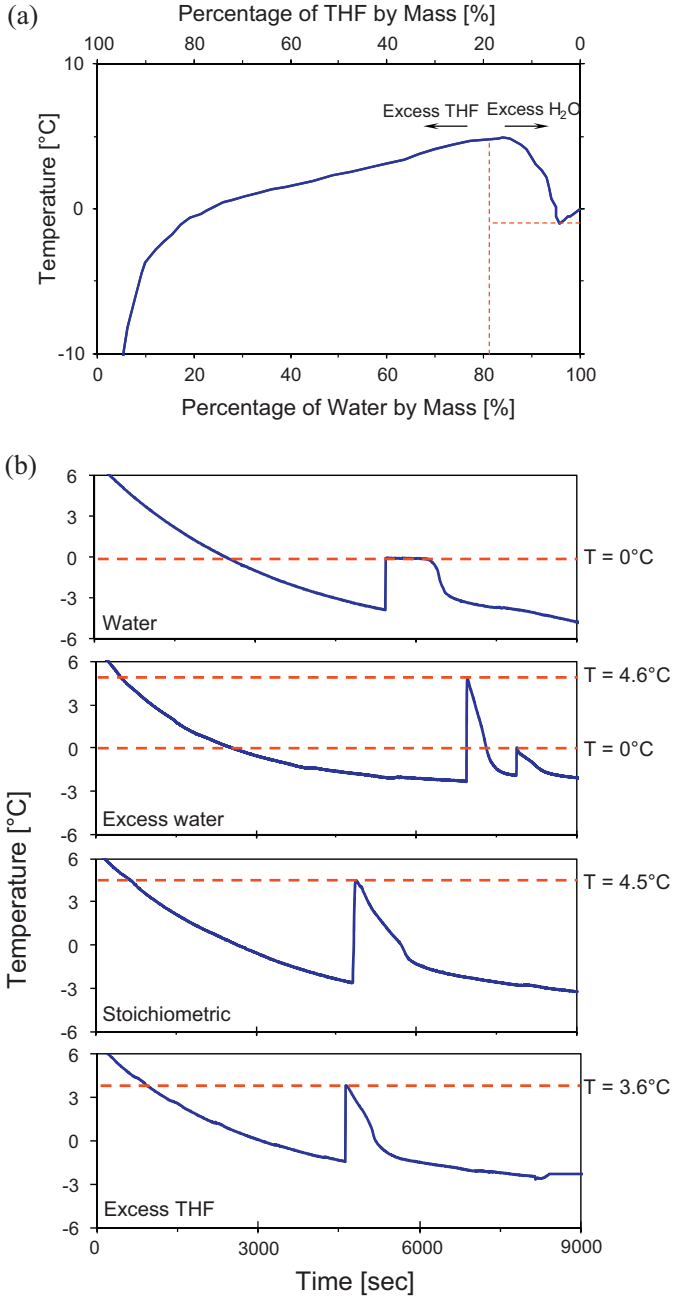

Fig. 3. Phase transformation. (a) Stability temperature for THF–water mixtures at atmospheric pressure. (b) Typical temperature–time signatures for tap water, THF solution with excess water ($90H_2O$:10THF), stoichiometric mixture 100% hydrate ($81H_2O$:19THF), and THF solution with excess THF ($40H_2O$:60THF).

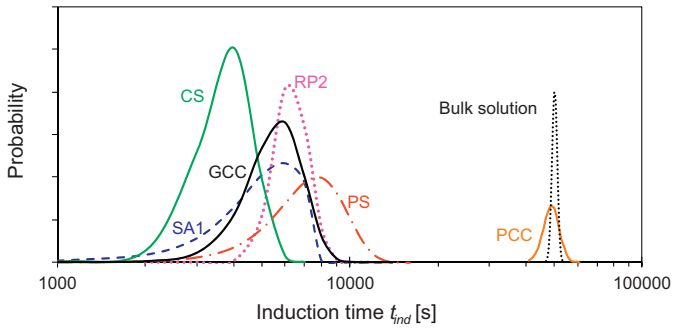

Fig. 4. Effect of mineral grain characteristics on induction time. Kaolinite (SA1), kaolinite (RP2), precipitated silt (PS), crushed silt (CS), ground $CaCO_3$ (GCC), precipitated $CaCO_3$ (PCC).

4.2. The effect of mechanical vibration on nucleation

The effect of mechanical vibration on nucleation is explored by plotting the data on tripartite plots so that imposed sinusoidal vibration frequency, displacement, velocity, and acceleration are shown at once (Fig. 5). The measured data were sorted from short to long induction times, and the boundary between short induction times (crosses) and long induction times (circles) was gradually displaced to attain maximum data discrimination. Results obtained with both water-to-ice and THF solution-to-hydrate transformations show that the boundary from short-to-long induction times is parallel to iso-acceleration lines; thus, acceleration is the best predictor of reduced induction time.

A characteristic acceleration threshold is apparent in Fig. 5. This is further explored in Fig. 6 where induction times are plotted versus peak acceleration. The solid line represents the mean induction time $\mu(t_{ind})$ and dashed lines represent the one standard deviation $\pm\sigma(t_{ind})$ band in induction times measured for specimens without vibration as the control group. The induction time decreases when the peak acceleration exceeds $\sim$10 m/s^2. Histograms of short and long induction times for high and low accelerations show that mechanical vibration does not suppress induction time variability. Hydrate nucleation under quiescent conditions shows decreased induction times and variability (in linear scale) when the system is driven further into stability conditions [8].

Several hypotheses have been advanced to explain the role of agitation on nucleation. Some suggest that mechanical agitation enhances nucleation by altering incipient nuclei to favor crystallization sites [28,39]. Others consider that mechanical agitation causes transient inhomogeneous energy distribution and high energy regions favor nucleation [1].

At the molecular scale, agitation must cause enough relative displacement among neighboring molecules to facilitate nucleation and the formation of a new structure. Let us idealize molecular scale interactions as a damped, single degree of freedom with a linear spring k, mass m, and dashpot η. The motion that the second molecular layer experiences $y_{m(t)}$ is related to the motion imposed on the first layer $y_{b(t)} = A\cos(\omega t)$ as

$$y_{m(t)} = H \times y_{b(t)}, \tag{2}$$

where the transfer function H represents the intermolecular response function. The equation of motion follows Newton's second law:

$$m\frac{\partial^2 y_{m(t)}}{\partial t^2} + \eta\frac{\partial(y_{m(t)} - y_{b(t)})}{\partial t} + k(y_{m(t)} - y_{b(t)}) = 0 \tag{3}$$

The combination of Eqs. (2) and (3) renders:

$$H = \frac{\omega\eta - k}{\omega^2 m + \omega\eta - k}. \tag{4}$$

Thus, the maximum relative displacement δ become

$$\delta = |y_{m(t)} - y_{b(t)}|_{\max} = |(H-1)y_{b(t)}|_{\max} = \frac{A}{1 + \frac{\eta}{\omega m} - \left(\frac{\omega_r}{\omega}\right)^2}, \tag{5}$$

where the resonant frequency $\omega_r{}^2 = k/m$. The excitation frequencies in this study are much lower than molecular resonance/relaxation frequencies, $\omega/\omega_r \ll 1$. In this regime, the relative displacement between contiguous molecular layers δ/A scales with ω^2. This is in

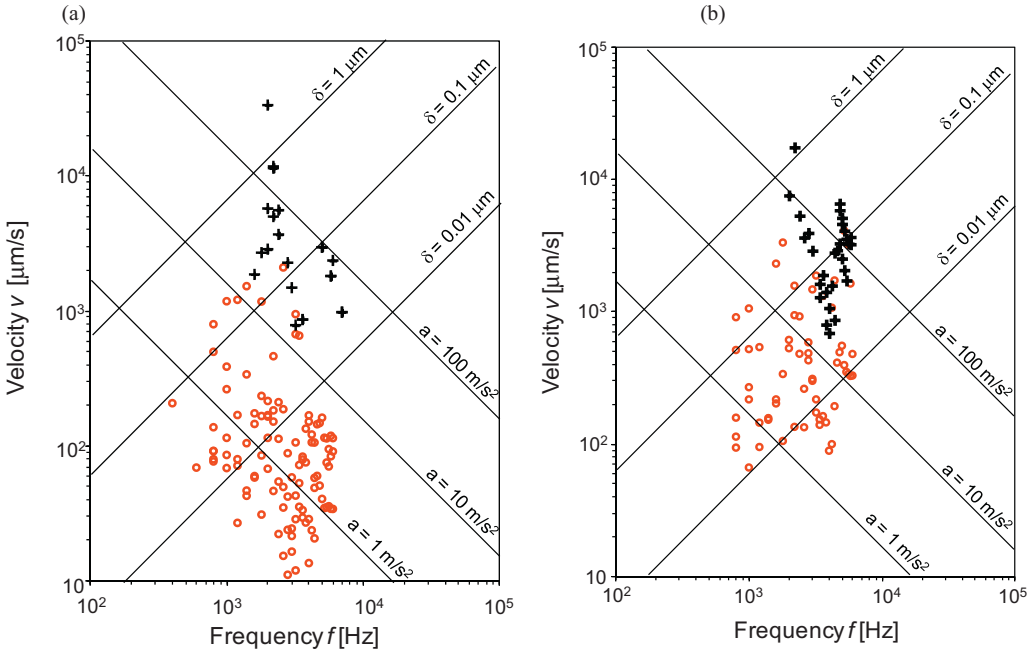

Fig. 5. Experimental results in tripartite: (a) water to ice and (b) stoichiometric THF–water to hydrate transition. Induction times are represented by symbols: in (a) crosses are results of $t_{ind} < 2500$ s and circles are results of $t_{ind} > 2500$ s; in (b) crosses are results of $t_{ind} < 5000$ s and circles are results of $t_{ind} > 5000$ s.

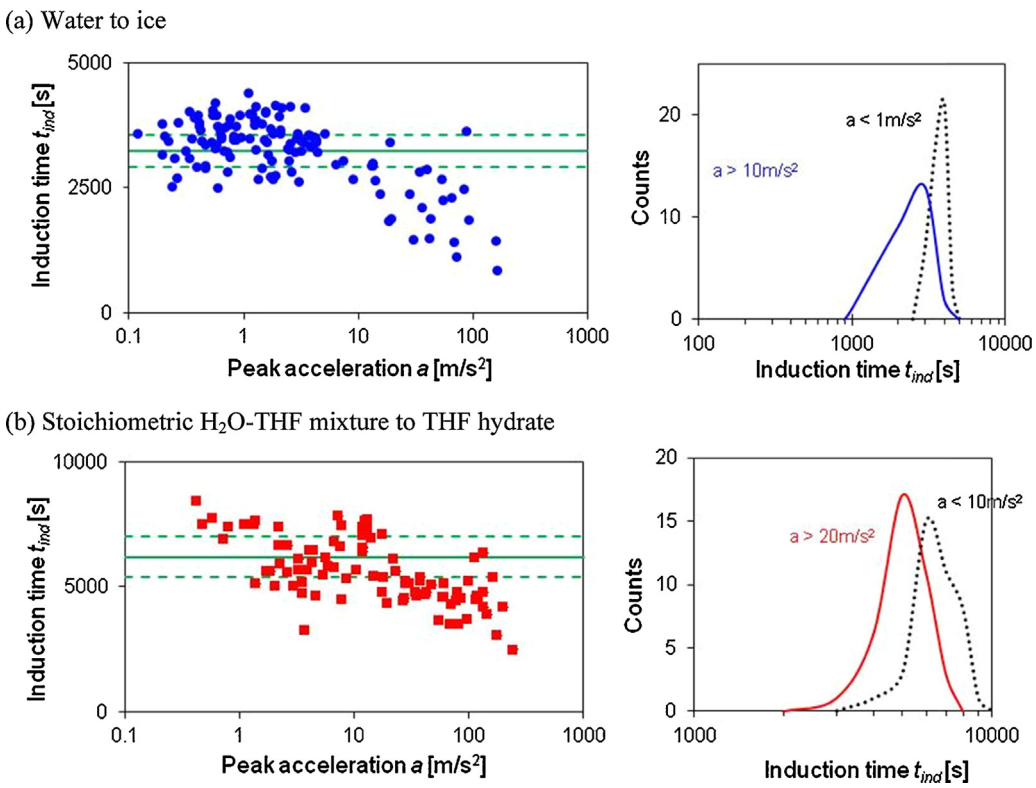

Fig. 6. Experimental results: Induction time t_{ind} versus peak acceleration a. Cases: (a) tap water and (b) stoichiometric mixture ($81H_2O$:19THF) 100% hydrate. Discrete points are experimental results obtained with mechanical vibrations. As a reference, the mean and standard deviation values of 16 specimens without vibration are shown as solid and dashed lines.

agreement with experimental results in Fig. 5 that show acceleration $a = A\omega^2$ as the key vibration characteristic that affects induction time.

5. Conclusions

Solid phase hydrate formation exhibits induction time, supercooling, and transformation temperature depression. Nucleation is inherently stochastic and experimental results should be expressed in statistical form.

The induction time of THF hydrate formation in various types of mineral suspensions follows a log-normal distribution. Nucleation is favored in the presence of most minerals. Mineral surface properties affect the induction time and the degree of supercooling but do not change the equilibrium temperature during phase transformation. Mineralogy and fluid–mineral interaction (i.e., contact angle and interfacial tension) are more important than particle size and sediment porosity.

Mechanical vibration facilitates nucleation but it does not suppress the inherent stochastic nature of nucleation.

The tripartite analysis of experimental results reveals that acceleration is a better discriminator between short and long induction times than vibration frequency, amplitude, or velocity. Experimental results suggest that nucleation is prompted when the imposed acceleration exceeds ~10 m/s^2. Relative molecular displacement emerges as the underlying mechanism. Thus, boundary layer shear and pore-scale turbulence in steady sate flow conditions should favor nucleation.

Acknowledgements

Support for this research was provided by the Joint Industry Project for Methane Hydrate administered by Chevron under contract DE-FC26-01NT41330 from the U.S. Department of Energy to Georgia Tech. Additional funds were from the Goizueta Foundation. We also wish to acknowledge the support of the Korea Institute of Geoscience and Mineral Resources and the Gas Hydrate Research and Development Organization (GHDO) of the Ministry of Trade, Industry, and Energy, Republic of Korea.

Appendix A. Supplementary data

Supplementary data associated with this article can be found, in the online version, at doi:10.1016/j.fluid.2014.07.006.

References

[1] J.W. Mullin, Crystallization, Butterworth-Heinemann, Jordan Hill, Oxford, 2001.
[2] E.D. Sloan, F. Fleyfel, A molecular mechanism for gas hydrate nucleation from ice, AIChE J. 37 (9) (1991) 1281–1292.
[3] P. Englezos, S. Hall, Phase equilibrium data on carbon dioxide hydrate in the presence of electrolytes, water soluble polymers and montmorillonite, Can. J. Chem. Eng. 72 (5) (1994) 887–893.
[4] P. Skovborg, H.J. Ng, P. Rasmussen, U. Mohn, Measurement of induction times for the formation of methane and ethane gas hydrates, Chem. Eng. Sci. 48 (3) (1993) 445–453.
[5] E.D. Sloan, C.A. Koh, Clathrate Hydrates of Natural Gases, 3rd ed., CRC Press, Boca Raton, 2008.
[6] P.R. Bishnoi, V. Natarajan, Formation and decomposition of gas hydrates, Fluid Phase Equilib. 117 (1) (1996) 168–177.
[7] V. Natarajan, P. Bishnoi, N. Kalogerakis, Induction phenomena in gas hydrate nucleation, Chem. Eng. Sci. 49 (13) (1994) 2075–2087.
[8] K. Lee, S.-H. Lee, W. Lee, Stochastic nature of carbon dioxide hydrate induction times in Na-montmorillonite and marine sediment suspensions, Int. J. Greenh. Gas Control 14 (2013) 15–24.
[9] E. Sloan, C. Koh, A. Sum, A. Ballard, G. Shoup, N. McMullen, J. Creek, T. Palermo, Hydrates: state of the art inside and outside flowlines, J. Pet. Technol. 61 (12) (2009) 89–94.
[10] C.A. Koh, A.K. Sum, E.D. Sloan, Gas hydrates: unlocking the energy from icy cages, J. Appl. Phys. 106 (6) (2009), 061101-061101-061114.

[11] B. Tohidi, J. Yang, M. Salehabadi, R. Anderson, A. Chapoy, CO_2 hydrates could provide secondary safety factor in subsurface sequestration of CO_2, Environ. Sci. Technol. 44 (4) (2010) 1509–1514.
[12] J.W. Jung, D.N. Espinoza, J.C. Santamarina, Hydrate bearing sediments: CH_4-CO_2 replacement, J. Geophys. Res. 115 (2010) B10102, http://dx.doi.org/10.1029/2009JB000812.
[13] A. Vysniauskas, P.R. Bishnoi, A kinetic study of methane hydrate formation, Chem. Eng. Sci. 38 (7) (1983) 1061–1072.
[14] P.V. Hobbs, Ice Physics, Clarendon Press, Ice Physics: Oxford, 1974.
[15] S.W. Young, R.J. Cross, The mechanical stimulus to crystallization, J. Am. Chem. Soc. 33 (8) (1911) 1375–1388.
[16] S. Al-Adel, J.A.G. Dick, R. El-Ghafari, P. Servio, The effect of biological and polymeric inhibitors on methane gas hydrate growth kinetics, Fluid Phase Equilib. 267 (1) (2008) 92–98.
[17] W. Lin, G.J. Chen, C.Y. Sun, X.Q. Guo, Z.K. Wu, M.Y. Liang, L.T. Chen, L.Y. Yang, Effect of surfactant on the formation and dissociation kinetic behavior of methane hydrate, Chem. Eng. Sci. 59 (21) (2004) 4449–4455.
[18] S.B. Cha, H. Ouar, T.R. Wildeman, E.D. Sloan, A third-surface effect on hydrate formation, J. Phys. Chem. 92 (23) (1988) 6492–6494.
[19] D. Riestenberg, O. West, S. Lee, S. McCallum, T.J. Phelps, Sediment surface effects on methane hydrate formation and dissociation, Marine Geol. 198 (1–2) (2003) 181–190.
[20] H.S.U.H. Ting, W.L. McCabe, Supersaturation and crystal formation in seeded solutions, Ind. Eng. Chem. 26 (11) (1934) 1201–1207.
[21] B.M. Clennell, M. Hovland, J.S. Booth, P. Henry, W.J. Winters, Formation of natural gas hydrates in marine sediments. 1. Conceptual model of gas hydrate growth conditioned by host sediment properties, J. Geophys. Res. 104 (B10) (1999) 22985–23003.
[22] N.H. Fletcher, Size effect in heterogeneous nucleation, J. Chem. Phys. 29 (3) (1958) 572–576.
[23] Y.P. Handa, D.Y. Stupin, Thermodynamic properties and dissociation characteristics of methane and propane hydrates in 70-.ANG.-radius silica gel pores, J. Phys. Chem. 96 (21) (1992) 8599–8603.
[24] B. Husowitz, V. Talanquer, Nucleation in cylindrical capillaries, J. Chem. Phys. 121 (16) (2004) 8021–8028.
[25] T.-H. Kwon, G.-C. Cho, J.C. Santamarina, Gas hydrate dissociation in sediments: pressure–temperature evolution, Geochem. Geophys. Geosyst. 9 (3) (2008) Q03019.
[26] K.K. Østergaard, R. Anderson, M. Llamedo, B. Tohidi, Hydrate phase equilibria in porous media: effect of pore size and salinity, Terra Nova 14 (5) (2002) 307–312.
[27] F. Restagno, L. Bocquet, T. Biben, Metastability and nucleation in capillary condensation, Phys. Rev. Lett. 84 (11) (2000) 2433–2436.
[28] J.W. Mullin, K.D. Raven, Influence of mechanical agitation on the nucleation of some aqueous salt solutions, Nature 195 (4836) (1962) 35–38.
[29] S.W. Young, Mechanical stimulus to crystallization in supercooled liquids, J. Am. Chem. Soc. 33 (2) (1911) 148–162.
[30] R.M. Barrer, A.V.J. Edge, Gas hydrates containing argon, krypton and xenon: kinetics and energetics of formation and equilibria, Proc. R. Soc. A: Math. Phys. Sci. 300 (1460) (1967) 1–24.
[31] H. Tajima, A. Yamasaki, F. Kiyono, Continuous formation of CO_2 hydrate via a Kenics-type static mixer, Energy Fuels 18 (5) (2004) 1451–1456.
[32] C. Akkermans, P. Venema, S. Rogers, A. van der Goot, R. Boom, E. van der Linden, Shear pulses nucleate fibril aggregation, Food Biophys. 1 (3) (2006) 144–150.
[33] K. Liang, G. White, D. Wilkinson, L.J. Ford, K.J. Roberts, W.M.L. Wood, Examination of the process scale dependence of l-glutamic acid batch crystallized from supersaturated aqueous solutions in relation to reactor hydrodynamics, Ind. Eng. Chem. Res. 43 (5) (2004) 1227–1234.
[34] J.Y. Lee, T.S. Yun, J.C. Santamarina, C. Ruppel, Observations related to tetrahydrofuran and methane hydrates for laboratory studies of hydrate-bearing sediments, Geochem. Geophys. Geosyst. 8 (2007) Q06003, http://dx.doi.org/10.1029/2006GC001531.
[35] T.S. Yun, J.C. Santamarina, C. Ruppel, Mechanical properties of sand, silt, and clay containing tetrahydrofuran hydrate, J. Geophys. Res. 112 (2007) B04106, http://dx.doi.org/10.1029/2006JB004484.
[36] V.R. Blackwell, Formation Processes of Clathrate Hydrates of Carbon Dioxide and Methane, California Institute of Technology, PhD Thesis, Pasadena, CA., 1999.
[37] S.-H. Park, G. Sposito, Do montmorillonite surfaces promote methane hydrate formation? Monte carlo and molecular dynamics simulations, J. Phys. Chem. B 107 (10) (2003) 2281–2290.
[38] D. Turnbull, B. Vonnegut, Nucleation catalysis, Ind. Eng. Chem. 44 (6) (1952) 1292–1298.
[39] T.P. Melia, W.P. Moffitt, Secondary nucleation from aqueous solution, Ind. Eng. Chem. Fundam. 3 (4) (1964) 313–317.